Determining the Specificity of Monoclonal Antibody HPT-101 to Tau-Peptides with Optical Tweezers

Tim Stangner,[†,*] Carolin Wagner,[†] David Singer,[‡] Stefano Angioletti-Uberti,[§] Christof Gutsche,[†] Joachim Dzubiella,[§,⊥] Ralf Hoffmann,[‡] and Friedrich Kremer[†]

[†]Department of Experimental Physics I, Leipzig University, Linnéstraße 5, D-04103 Leipzig, Germany, [‡]Center for Biotechnology and Biomedicine (BBZ), Institute for Bioanalytical Chemistry, Leipzig University, Deutscher Platz 5, D-04103 Leipzig, Germany, [§]Department of Physics, Humboldt University Berlin, Newtonstraße 15, 12489 Berlin, Germany, and [⊥]Soft Matter and Functional Materials, Helmholtz-Zentrum Berlin for Materials and Energy, Hahn-Meitner-Platz 1, 14109 Berlin, Germany

ABSTRACT Optical tweezers-assisted dynamic force spectroscopy is employed to investigate specific receptor–ligand interactions on the level of single binding events. In particular, we analyze binding of the phosphorylation-specific monoclonal antibody (mAb) HPT-101 to synthetic tau-peptides with two potential phosphorylation sites (Thr231 and Ser235), being the most probable markers for Alzheimer's disease. Whereas the typical interpretation of enzyme-linked immunosorbent assay (ELISA) suggests that this monoclonal antibody binds exclusively to the double-phosphorylated tau-peptide, we show here by DFS that the specificity of only mAb HPT-101 is apparent. In fact, binding occurs also to each sort of monophosphorylated peptide. Therefore, we characterize the unbinding process by analyzing the measured rupture force distributions, from which the lifetime of the bond without force τ_0, its characteristic length x_{ts}, and the free energy of activation ΔG are extracted for the three mAb/peptide combinations. This information is used to build a simple theoretical model to predict features of the unbinding process for the double-phosphorylated peptide purely based on data on the monophosphorylated ones. Finally, we introduce a method to combine binding and unbinding measurements to estimate the relative affinity of the bonds. The values obtained for this quantity are in accordance with ELISA, showing how DFS can offer important insights about the dynamic binding process that are not accessible with this common and widespread assay.

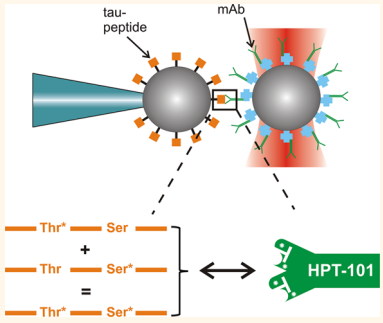

KEYWORDS: single-molecule measurements · ELISA · optical tweezers · dynamic force spectroscopy · specificity · affinity · Alzheimer's disease

Monoclonal antibodies (mAbs) were first produced *in vitro* by Köhler and Milstein[1] in 1975. However, their medical application in the late 1980s initially failed, since the treatment of patients with murine antibodies was often associated with allergic reactions and the induction of anti-drug antibodies.[2] Two decades of advances in genetic engineering changed this situation, and mAbs are nowadays widely used as medical agents (*e.g.*, in the treatment of cancer using antibody drug conjugates,[3−8] rheumatoid arthritis,[8] Crohn's disease, multiple sclerosis, prophylaxis for transplant rejection[2]). The key feature of mAbs-based therapies is the targeted administration of highly potent drugs in combination with the reduction of negative side-effects to healthy tissue due to so-called cross reactions. To achieve this goal, a high target selectivity (or specificity) of the used mAb is imperative,[4] meaning that the antibody must bind only to the disease-specific marker, whereas no cross reactivity to other tissue should occur.

Apart from their applications in drug delivery, mAbs are also being used and developed as diagnostic tools in immunohistochemistry[9,10] and flow cytometry.[11] In the context of neurodegenerative diseases (*e.g.*, Alzheimer's disease), when symptoms are heterogeneous or their initial manifestation is ambiguous and can be mistaken with that of other conditions,[12] the specificity of mAbs can be of invaluable help for the early detection of the disease.

In Alzheimer's disease the microtubule-associated tau protein becomes hyperphosphorylated and self-associates to form paired helical filaments (PHF). In a healthy brain tau promotes the assembly and stabilization of neuronal microtubules and plays

* Address correspondence to stangner@physik.uni-leipzig.de.

Received for review October 11, 2013 and accepted November 26, 2013.

Published online November 26, 2013
10.1021/nn405303u

a crucial role in neurogenesis and axonal transport as well as in axons' maintenance.[13−15] After the formation of these PHF−tau complexes, they aggregate in neurofibrillary tangles in the cortical brain areas, which are essential for cognitive function, and this is found to be one of the pathological characteristics of Alzheimer's disease.[15] In recent years, the physical and chemical properties of these tau aggregates have been intensively studied in simulations[16−19] and experiment.[14,20−23] However, a link between self-aggregation, phosphorylation pattern, and the cause as well as the progress of Alzheimer's disease is still missing.[10,24] Nonetheless, mAbs can be used for the histological detection of Alzheimer-specific phosphorylated tau-peptides and even to discriminate between different phosphorylation patterns. As for the drug delivery applications, a high target specificity of the antibody must be guaranteed in this case, too.

In a previous study[10] the phosphorylation-dependent mAb HPT-101 was produced, and its specificity to different synthetic tau-peptides was determined using the enzyme-linked immunosorbent assay (ELISA). Interestingly, these assays showed that mAb HPT-101 binds specifically only to the epitope of the double-phosphorylated peptide tau226−240[pThr231/pSer235] comprising the amino acids from position 231 to 236. Cross reactions to monophosphorylated peptides with the same amino acid sequence were not observed, although the epitope differs only by a single isolated phosphorylation site.[10]

Despite its outstanding performance in screening applications, a fundamental understanding of the dynamic binding process is not accessible with ELISA measurements, since it provides only a static, equilibrated picture. However, to comprehend the overall receptor−ligand interaction (*e.g.*, specificity of the mAb), more details about the binding kinetics are required. In this paper we demonstrate with the help of single-molecule analysis that cross reactions between the mAb HPT-101 and the monophosphorylated peptides tau226−240[pThr231] and tau226−240[pSer235] do occur. The receptor ligand bond is characterized with optical tweezers-assisted dynamic force spectroscopy (OT-DFS),[25−28] and kinetic bond parameters are extracted. Using the on-rate and off-rate from our measurements, we calculate the relative affinity of mAb HPT-101 to all three peptides (one double-phosphorylated, two monophosphorylated). The highest affinity is observed for the double-phosphorylated peptide, in accordance with ELISA measurements. Additionally, we propose a simple model to calculate the binding characteristics for the double phosphorylated peptide by combining the data from the monophosphorylated ones, providing a deeper understanding of the bond origin.

RESULTS AND DISCUSSION

mAb HPT-101 Shows Cross Reactivity: Binding Frequencies. To measure the interaction between the three different tau-peptides and the mAb HPT-101, we trap a single peptide-coated particle with our optical tweezers and bring it in the vicinity of the custom-made micropipet. This colloid is fixed on the tip of the pipet by capillary forces. Next, a second colloid covered with the mAb is captured and placed in close proximity of the immobilized bead on the pipet (inset in Figure 1). Using a custom-made LabView program, both particles are approached until a force of 5 ± 2 pN is reached and retracted with a distinct velocity after one second of contact time. If a bond has formed, the particle in the optical trap is displaced out if its equilibrium position until the rupture force is exceeded. At this force the bond breaks and the particle snaps back into its initial position (Figure 1).

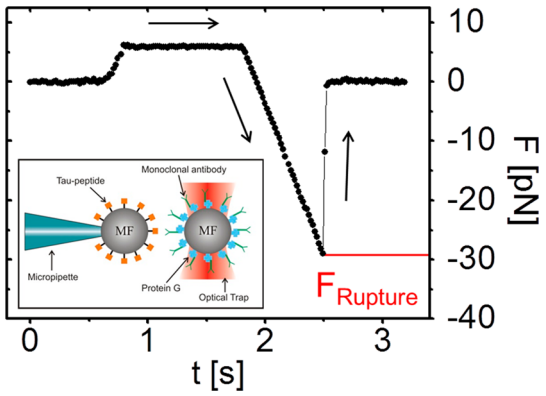

Figure 1. Temporal evolution of a typical approach−retraction cycle. To establish the binding, the colloids are approached toward each other until a force of 5 ± 2 pN is reached. After one second of contact they are pulled apart with a preset velocity. Due to the interaction between receptor and ligand, the particle in the optical trap is deflected from its equilibrium position, until the rupture of the binding can be observed (rupture force). (Inset) Experimental configuration. The particle coated with the mAb HPT-101 is kept in the optical trap. The mAbs are orientated by use of protein G. The particle covered with the respective tau-peptide is fixed at the tip of a micropipet by capillary forces.

In order to determine the relative binding frequencies h_B of the interaction between mAb HPT-101 and the tau-peptides tau[pThr231/pSer235], tau[pThr231], and tau[pSer235], we count the number of binding events in at least 30 approach−retraction cycles per colloid pair. For every interaction, five pairs of colloids have been investigated. Figure 2 shows the median binding frequency of each interaction. The error bars constitute the median standard deviation, which is caused by variances of the coating densities of individual colloids from one batch. Unspecific interactions (*e.g.*, interactions between particles covered with mAbs/peptide and uncoated particles as well as between particles covered with tau-peptides and particles coated only with protein G) are called background events. With a binding frequency below 2% they are found to be negligible. The number of detectable multiple rupture events is determined to be lower than 2% (see Materials and Methods).

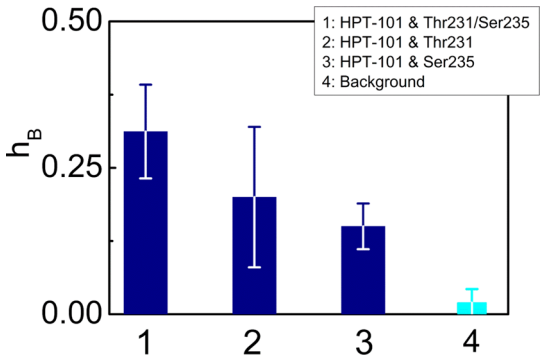

Figure 2. Median relative binding frequency h_B of mAb HPT-101 to the peptides (1) tau[pThr231/pSer235], (2) tau[pThr231], and (3) tau[pSer235]. For each interaction, five different pairs of colloids have been analyzed with regard to the binding frequency in 30−100 approach−retraction cycles. The error bars correspond to the median standard deviation.[41] The background value (4) constitutes interactions that are not caused by a binding between receptor and ligand.

The highest binding frequency of $h_B = 0.31 \pm 0.08$ is observed for the interaction of the mAb with the biphosphorylated peptide tau[pThr231/pSer235]. The monophosphorylated peptides tau[pThr231] and tau[pSer235] also bind with similar frequencies of 0.20 ± 0.12 and 0.15 ± 0.04, respectively. According to ELISA, mAb HPT-101 binds exclusively to the biphosphorylated peptide tau[pThr231/pSer235].[10] Although the highest binding frequency has been observed for this interaction, our single-molecule approach shows also an appreciable binding of mAb HPT-101 to the monophosphorylated peptides. Therefore, the supposed specificity of mAb HPT-101 to the biphosphorylated peptide cannot be confirmed by our approach. However, the binding frequency constitutes a measure for the relative on-rate only,[29] whereas the affinity of a bond is defined by the association constant K_a, which is the ratio between on- and off-rate. Thus, a full characterization requires the determination of the off-rate as well, using the procedure described in the next paragraph.

Dynamic Force Spectroscopy: Determining Bond Parameters. For the purpose of determining the off-rate k_{off} and the other binding parameters, we performed DFS measurements. Therefore, the interactions between the mAb HPT-101 and the three peptides, each having a different phosphorylation pattern, are analyzed on the level of single binding events. The loading rate is varied in the range 24−98 pN s^{-1} (with an average error of 12%) for all measurements.

Figure 3a depicts the respective rupture force distributions at a loading rate of 56 ± 7 pN s^{-1} containing at least 100 binding events for each case. The bin size b was calculated using Scott's rule:[30] $b = 3.5\sigma/(n)^{1/3}$ in which σ is the standard deviation and n the number of rupture events. It is evident from the data that the median rupture force is clearly shifted to lower values by reducing the number of phosphorylation sites. The biphosphorylated peptide tau[pThr231/pSer235] (Figure 3a, top), for which the highest binding frequency (0.31 ± 0.08) has been determined, shows also the highest median rupture force of 42.1 ± 2.0 pN. The rupture force ($F_{median} = 25.5 \pm 1.5$ pN) of the peptide carrying a phosphorylation at Thr231 (Figure 3a, middle) follows the trend of the recorded binding frequencies and decreases by a factor of almost 2. The weakest interaction ($F_{median} = 7.2 \pm 1.0$ pN) occurs between mAb HPT-101 and tau[pSer235] (Figure 3a, bottom), which is in accordance with our binding frequency measurements, too. By changing the loading rate a similar trend is observed. The rupture force distributions show a shift according to the dependence of the median rupture force on the natural logarithm of the loading rate (data not shown), as captured by the DHS model.

To extract binding parameters, we analyze our experimental data in light of the Dudko, Hummer, and Szabo (DHS) model. Therefore, we calculate the discrete function $\tau(F)$ from the rupture force distribution following the instructions as described in Materials and Methods for all three loading rates using eq 8. This procedure is applied to the interaction between mAb HPT-101 and the biphosphorylated peptide tau[pThr231/pSer235] and the monophosphorylated peptide tau[pThr231], respectively. Due to the shape of the rupture-force distribution, the small force close to the resolution limit of our setup, and the outliers around 40 pN, the transformation into $\tau(F)$ of the binding between mAb HPT-101 and the peptide tau[pSer235] cannot be done using eq 8. For this case, we use eq 9, omitting rupture forces above 30 pN. Figure 3b shows that the force-dependent lifetime $\tau(F)$ collapses for all three loading rates onto a single master curve, independent of the used peptide. This behavior is expected from the DHS theory.[31] The solid lines correspond to the fit using eq 6 for $\upsilon = 0.5$. As can be seen from the plots, good agreement between data and theoretical prediction is achieved. For reasons of clarity we present only the fit for $\upsilon = 0.5$, since only minor deviations occurred for $\upsilon = 0.66$.

Figure 4 provides an overview of the obtained fit parameters obtained for $\upsilon = 0.5$. For ease of comparison the obtained values for the relative binding frequency h_B (Figure 2) and the median rupture force $\langle F \rangle_{median}$ (Figure 3a) are shown again. The longest bond lifetime with $\tau_0 = 12.7 \pm 0.8$ s is given by the interaction between mAb HPT-101 and the peptide tau[pThr231/pSer235]. This value is 1 order of magnitude larger compared to the lifetime of peptide tau[pThr231] ($\tau_0 = 1.55 \pm 0.10$ s). Resulting from this, the more persistent bond reveals also the highest values for the binding length ($x_{ts} = 0.54 \pm 0.03$ nm) as well as for the free activation energy ($\Delta G = 6.4 \pm 1.3\ k_BT$). For these two latter cases the binding of the mAb to the

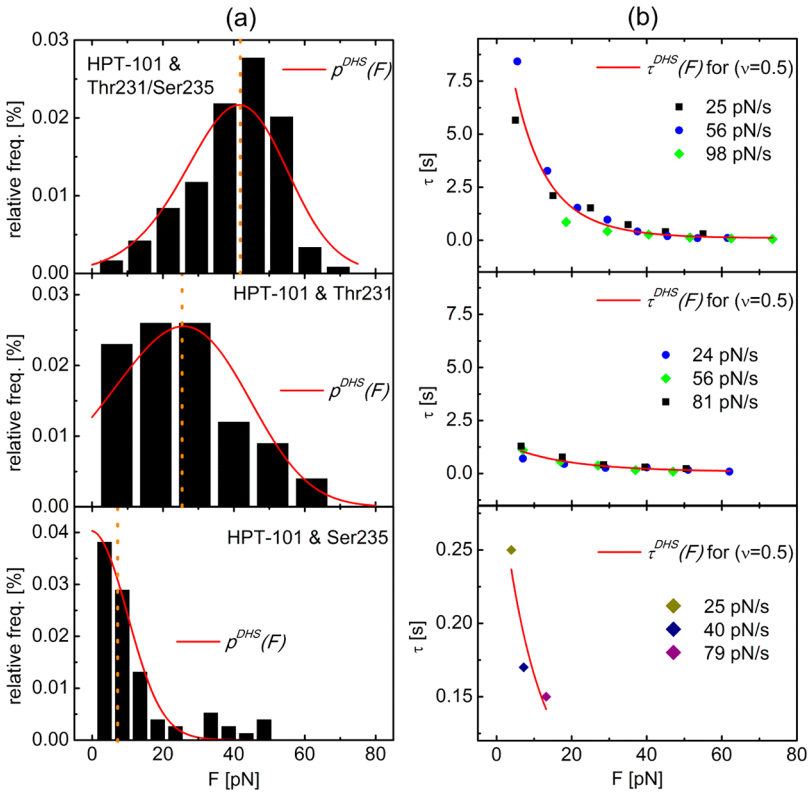

Figure 3. (a) Rupture-force histograms of the interaction between mAb HPT-101 and the peptides tau[pThr231/pSer235] (top), tau[pThr231] (middle), and tau[pSer235] (bottom) at a loading rate of 56 ± 7 pN s^{-1}. Each histogram is based on more than 100 rupture events. The dashed lines illustrate the median rupture forces. The red lines correspond to the theoretical distribution of rupture forces (eq 7) for the parameters obtained by fitting $\tau_{DHS}(F)$ to the Dudko, Hummer, and Szabo (DHS) function. (b) Force-dependent lifetime of the interaction from the left side. For each interaction, three different loading rates are given. For the interaction of mAb HPT-101 with tau[pThr231/pSer235] (top) and tau[pThr231] (middle), the discrete $\tau(F)$ functions have been calculated for each loading rate according to eq 8 from the respective rupture-force distribution. $\tau(F)$ collapses for all loading rates onto a single master curve, as predicted by the DHS theory. Due to the shape of the rupture-force distribution, the force-dependent bond lifetime was calculated using eq 9 for the binding between mAb HPT-101 and tau[pSer235] (right, bottom). The discrete functions for each interaction have been fitted to $\tau_{DHS}(F)$ (eq 6) for $\upsilon = 0.5$ (red line) in order to determine the binding parameters τ_0, x_{ts}, and ΔG.

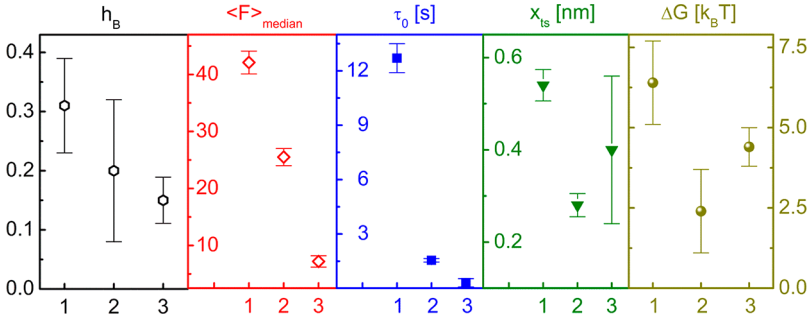

Figure 4. Relative binding frequency h_B, median rupture force $\langle F \rangle_{median}$, lifetime at zero applied force τ_0, characteristic length x_{ts}, and free activation energy ΔG for the interaction between mAb HPT-101 and the tau-peptides (1) tau[pThr231/pSer235], (2) tau[pThr231], and (3) tau[pSer235] according to the fit of eq 6 ($\upsilon = 0.5$), respectively. For the purpose of a better comparison the relative binding frequency is shown again. The interaction between mAb HPT-101 and the double-phosphorylated peptide tau[pThr231/pSe235] shows the highest bond lifetime, followed by the peptide carrying a phosphorylation at Thr231. The shortest lifetime is represented by the interaction between mAb HPT-101 and tau[pSer235]. For x_{ts} no such trend can be observed within the range of experimental accuracy. The relative binding frequency and the median rupture force follow the trend observed for τ_0, meaning that the highest values are obtained for the binding between HPT-101 and the peptide tau[pThr231/pSer235].

peptide phosphorylated at Thr231 yields x_{ts} = 0.28 ± 0.03 nm and ΔG = 4.4 ± 0.6 k_BT. The interaction between mAb HPT-101 and the monophosphorylated peptide tau[pSer235] shows the weakest interaction with a bond lifetime of τ_0 = 0.31 ± 0.23 s and potential depth of ΔG = 2.4 ± 1.3 k_BT. Only the binding length (x_{ts} = 0.40 ± 0.16 nm) is comparable to the other ones. In essence, the trend detected for the binding

frequencies is reproduced, meaning that the strongest bond occurs for mAb HPT-101 and tau[pThr231/pSer235], followed by the two monophosphorylated peptides tau[pThr231] and tau[pSer235], respectively.

Binding of the Double-Phosphorylated Peptide Recalculated from Data of the Monophosphorylated Ones. Considering that each monophosphorylated peptide contains the complementary part of the epitope of the double-phosphorylated peptide, we propose that the binding of mAb HPT-101 to the peptide tau[pThr231/pSer235] can be described as the sum of the interactions of mAb HPT-101 with tau[pThr231] and tau[pSer235], respectively. This assumption is supported by the fact that adding up the ΔG values from the monophosphorylated cases results in approximately the free activation energy of tau[pThr231/pSer235] as derived in the previous section. Following this idea, we try to gain some qualitative insights into the binding strength of the double-phosphorylated peptide to the mAb by assuming that binding occurs *via* formation of two single bonds. Each of these independent bonds comes from the binding of the antibody at the two distinct phosphorylation sites, an assumption that becomes true in the limit where the two sites are far apart.

We now interpret this hypothesis within the DHS model. In the latter, a bond is described by a single coordinate x moving stochastically on the potential:

$$\beta V(x) = \begin{cases} \frac{1}{2}k_m x^2 & \text{if } x < x_{ts}; \\ -\infty & \text{if } x > x_{ts} \end{cases} \quad (1)$$

Equation 1 represents the potential energy of a spring with elongation x, the spring being perfectly harmonic up to the limit elongation x_{ts}, when it breaks. k_m is thus the spring constant for the respective interaction. Within this model, one has the following definition for the free-energy barrier:

$$\beta\Delta G = \frac{1}{2}k_m(x_{ts})^2 \quad (2)$$

Kramers' equation[32] gives the mean-free-passage time (*e.g.*, the bond lifetime) at zero applied force as

$$\tau_0 = \frac{(2\pi)^{1/2}}{D k_m^{3/2} x_{ts}} \exp(\beta\Delta G) \quad (3)$$

where D is the diffusion coefficient for the variable describing the bond dissociation. Including the effect of a pulling force, the DHS model uses eqs 1−3 to derive eq 6, which gives the distribution of rupture times and hence, *via* eq 7, the distribution of rupture forces. τ_0, x_{ts}, and ΔG are the only system-dependent quantities entering in the DHS formula. Under our initial assumption of two independent binding sites, these quantities can be calculated for the interaction between mAb HPT-101 and tau[pThr231/pSer235] from the values of mAb HPT−101/tau[pThr231] and mAb HPT−101/tau[pSer235] alone. First of all, since each binding is treated as independent, the value of the molecular spring constant k_m for the single bond at each phosphorylation site can be calculated by inverting eq 2 from the known ΔG values for two monophosphorylated peptides. These two values must be combined into an effective spring constant for the double bond. As described in the Materials and Methods the force−time curves for the interaction of the mAb with the doubled phosphorylated peptide contain only single binding events. This suggests that both bonds stretch and break together, pointing to parallel loading of the force, resulting in $k_{pThr231/pSer235} = k_{pThr231} + k_{pSer235}$. Within the same assumption, we set $x_{ts}^{pThr231/pSer235} = \min(x_{ts}^{pThr231}, x_{ts}^{pSer235})$, because the double bond breaks as soon as the shorter single bond does. When the two bonds are independent, then each breaks at its own intrinsic maximum length x_{ts}. Once one of the two bonds is dissociated, the applied force must be sustained entirely by the remaining one, which breaks immediately. If this second event is fast (in our setup faster than $t < 16$ ms), the rupture of the "double bond" will be effectively identified as a single rupture event, as shown by the experimental data (Figure 1).

The obtained values for x_{ts} and ΔG can be used to calculate τ_0 for the binding of mAb HPT-101 to the doubled phosphorylated peptide. For this purpose, we assume that the diffusion coefficient D in eq 3 is independent of the particular molecular construct. Thus, τ_0 is calculated directly from the same equation since the ratio of τ_0's for interaction of mAb HPT-101 with the three different peptides now depends only on ΔG and x_{ts}, which we calculated previously (see Dynamic Force Spectroscopy section). Combining the obtained values for τ_0, x_{ts}, and ΔG with eqs 6 and 7 (see Materials and Methods), we obtain $p(F)$ within the independent binding assumption.

Figure 5 shows the comparison of our model (red, dashed curve) to the direct fitting of the experiments for the double-phosphorylated peptide and mAb HPT-101 with the DHS theory (black, solid curve). The position of the peak is well predicted, whereas the width of the distribution is broader (and thus its height necessarily lower, since this must follow from the normalization constraint on $p(F)$). Given that there are no fitting parameters in our model, the agreement is overall decent, supporting the fact that at least some features of the double-phosphorylated peptide binding are recovered from data on the monophosphorylated ones. Curiously, we see that ΔG calculated from this simplified model is lower compared to the measured one (5.5 k_BT *vs* 6.4 k_BT). Since ΔG is related to the strength of the bond, this means that our assumption of two independent single bonds underestimates the strength of the double-phosphorylated construct.

In order to correct the discrepancies in distribution width and in the calculated ΔG values, more

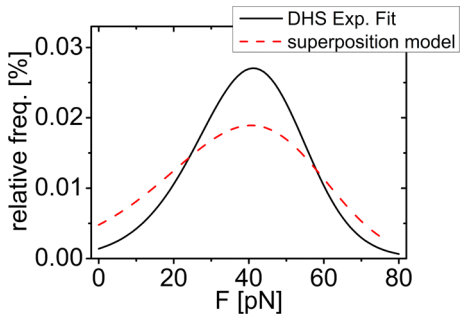

Figure 5. Comparison of our superposition model to predict the binding of the double-phosphorylated peptide using only data on the monophosphorylated ones (red, dashed curve) with direct fitting of the experimental data using the DHS theory (black, solid curve). The values of τ_0, x_{ts}, and ΔG for the calculation are taken from our dynamic force spectroscopy measurements. Clearly, our model well reproduces the position of the peak, whereas its width (and hence its height, given the normalization constraint) is overestimated, pointing to possible interactions between the two binding sites in determining the binding.

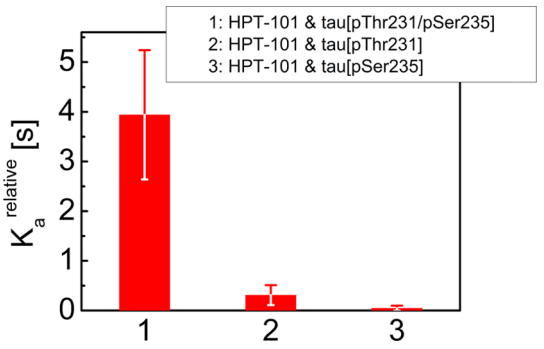

Figure 6. Relative affinities K_a^{rel} of the binding of mAb HPT-101 to the tau-peptides (1) tau[pThr231/pSer235], (2) tau-[pThr231], and (3) tau[pSer235] ($v = 0.5$). K_a^{rel} is the product of the lifetime without force τ_0 and the binding frequency h_B and is proportional to the association constant of the respective complex. The error bars are given by the propagation of the uncertainty of τ_0 and h_B. The highest relative affinity is obtained for the mAb HPT−101/tau[pThr231/pSer235] system, followed by the peptide phosphorylated at Thr231. The weakest affinity is observed for the interaction between mAb HPT-101 and the monophosphorylated peptide tau[pSer235]. This result is in accordance with ELISA.

complicated descriptions considering possible interactions between the phosphorylation sites (*e.g.*, correlations between the states of the two bonds) are necessary. For example, we assume in our analysis that each bond has an intrinsic stiffness (measured by $k_{pThr231}$ and $k_{pSer235}$, respectively), but stretching of one of the two bonds might lead to a change in the stiffness of the other. Furthermore it has to be mentioned that the real path leading to bond breaking involves many different coordinates (in principle up to $3N$, N being the total number of atoms in the system). Coarse-graining, *e.g.*, reducing the dimensionality of the problem, works because most of these coordinates are irrelevant in describing the overall features of the bond-breaking process, whereas a few selected ones play a bigger role. In our simplified model presented here (and more generally in the discussion of the DHS results), we assume the bond length to be a good coordinate, but others such as the angle between the peptide backbone and the pulling direction, or the torsional angle between the planes of the two epitopes with the backbone of the peptide, could also be important. Nonetheless, the fact that we recover a decent agreement with our simple model despite all assumptions we made is indeed an important indication that the mechanistic picture we provide does capture the main aspects of the bond-breaking process, although a full quantitative agreement with experimental data requires accounting for the possible effects previously described.

Relative Affinity from Single-Molecule Data Confirms ELISA Measurements. After assessing the binding frequency and off-rate by measuring the interaction between mAb HPT-101 and the three different peptides in molecular terms, we compare our single-molecule approach to the results obtained by immunochemical investigations (ELISA). Therefore we calculate the association constant K_a, which is defined as the ratio of on-rate and off-rate. The dissociation rate follows directly from the DFS measurements by the relation $k_{off} = \tau_0^{-1}$. The on-rate k_{on} is related to the binding frequency h_B in the following way: Neglecting the dissociation process, the mass action law reads as

$$\frac{d[RL]}{dt} = k_{on}[R][L] \tag{4}$$

with [RL] being the number of formed receptor−ligand complexes in a certain time dt, [R] and [L] being the receptor and ligand concentration, respectively. For the following calculations [RL] equals the binding frequency h_B. By assuming that the surface coverage of the different microparticles is identical, the product [R][L] becomes a constant. However this assumption is not totally fulfilled, as can be seen from the error bars in Figure 2. The incubation time dt is set as one second (see relative binding frequency measurements). It subsequently follows that the on-rate is directly proportional to the binding frequency. Finally the relative affinity is given by

$$K_a^{rel} = h_B\tau_0 \propto k_{on}\tau_0 = \frac{k_{on}}{k_{off}^0} = K_a \tag{5}$$

The relative affinity of mAb HPT-101 to the different types of peptides is shown in Figure 6. It is evident that the interaction between the mAb and the biphosphorylated peptide shows the highest relative affinity (K_a^{rel} = 3.94 ± 1.3 s). Compared to this, the affinity of tau[pThr231] (K_a^{rel} = 0.31 ± 0.20 s) is decreased by a factor of 10 and that of tau[pSer235] (K_a^{rel} = 0.047 ± 0.050 s) by a factor of almost 100. This strong splitting is mainly caused due to the large differences in τ_0 since binding frequencies differ only slightly. By multiplying both quantities to get the relative affinity, this effect is enhanced strongly, resulting in the highest specificity

of mAb HPT-101 to the biphosphorylated peptide. In a previous study[10] the affinity of mAb HPT-101 was investigated against the same peptides as we use in our measurements. It was found that mAb HPT-101 binds exclusively to the doubled phosphorylated peptide. Binding to other epitopes were not observed. From this we conclude that our single-molecule approach is consistent with this ELISA measurement.

Furthermore, the aforementioned cross reactivity indicates that not only a distinct phosphorylation pattern contributes to the receptor ligand bond but also the surrounding amino acids, as they may slightly influence the free energy landscape of the epitope. By assuming that the binding is dominated by the electrostatic interactions between antibody and the negatively charged phosphorylation sites of the peptide it can be concluded that the cross reactions between mAb HPT-101 and tau[pThr231] as well as tau[pSer235], respectively, are too weak to be detected by ELISA.

However, it has to be mentioned that the absolute numbers for the affinity resulting from ELISA and our method cannot be directly compared, since in the immunochemical approach the mAb molecules diffuse freely in solution and only the peptide is immobilized. In the optical tweezers measurement both binding partners are attached on microparticle surfaces and are brought into contact. Nonetheless the agreement between both methods remains valid.

CONCLUSIONS

In the present study, we investigated the interactions between mAb HPT-101 and tau-peptides with different phosphorylation patterns on a single-molecule level. In contrast to ELISA measurements, we observe with our dynamic approach that cross reactions between the mAb HPT-101 and the monophosphorylated peptides tau226−240[pThr231] and tau226−240[pSer235] do occur, meaning that the antibody binds to every used peptide type and not exclusively to the peptide tau-[pThr231/pSer235]. However, the specific binding to the double-phosphorylated peptide exhibits the longest lifetime and the highest free energy of activation. Furthermore, we introduced a method to determine the relative affinity from the single-molecule experiments. The values extracted using this procedure reveal that the binding to the double-phosphorylated peptide has the highest affinity, in accordance with the ELISA measurement. The measured binding frequencies for the two mutations tau226−240[pThr231] and tau226−240[pSer235] are close to that of the double-phosphorylated peptide, demonstrating that for these interactions the large deviations in the final relative affinity are dominated by the unbinding process, with rates differing by orders of magnitude between respective peptides. Finally, information extracted from the theoretical analysis of our measurements allow us to propose a simple model that combines data from the monophosphorylated peptides to predict the unbinding process of the double-phosphorylated one, providing a deeper understanding of the bond origin.

In brief, single-molecule force spectroscopy can help to increase the target specificity of mAbs since cross reactions to epitopes with a similar amino acid sequence can be detected and characterized, even if they are not observed in commonly used ensemble techniques. This precise knowledge might be of fundamental interest in the development and optimization of future therapeutic/diagnostic antibodies that can be used in human medicine.

MATERIALS AND METHODS

Sample Preparation. *Tau-Peptides and Monoclonal Antibodies.* The tau-peptides were synthesized by solid-phase peptide synthesis as previously published.[10] For the following experiments we use three different tau-peptides, each having a different phosphorylation pattern: double phosphorylated tau226−240[pThr231/pSer235] and two monophosphorylated, tau226−240[pThr231] and tau226−240[pSer235], peptides. Phosphorylation sites at Thr231 and Ser235 are found to be the most probable markers in Alzheimer's disease.[33] Each peptide type was N-terminally elongated with a cysteine residue containing a thiol group for covalent coupling of the peptides to beads by maleimide chemistry. The peptides were purified by reversed-phase high-performance liquid chromatography (RP-HPLC). The purity was determined by analytical RP-HPLC, and the correct mass was confirmed by mass spectrometry (MALDI-TOF-MS). mAb HPT-101 was produced in house.[10] Specific binding to the doubled phosphorylated peptide was proven by ELISA and Western blot, whereas no significant binding to the two monophosphorylated peptides as well as to the non-phosphorylated peptide was detected.[10]

Coating of Microparticles. For the measurements two types of colloids are prepared. The first type is coated with the tau-peptide, whereas the second is surface-functionalized with the mAb HPT-101 oriented by the use of protein G. All preparations are performed as previously published.[28] In detail the three different peptides were bound to maleimide-activated melamine resin (MF) particles (10 wt %, diameter 2.31 μm, Microparticles Berlin) in separate preparations. In addition, 2 μL of the respective peptide solution (peptide concentration c = 1.3 mg mL^{-1}, dissolved in phosphate-buffered saline (PBS)) was mixed with one equivalent of tris(2-carboxyethyl)phosphine and coupled *via* the thiol group to the colloids (25 μL). After 45 min of incubation, the colloids were washed with phosphate buffer containing 10 mmol L^{-1} cysteine and stored in the same solution at 4 °C. The mAb HPT-101 was oriented and connected to carboxylated MF microparticles (10 wt %, diameter: 2.31 μm, Microparticles Berlin) in a two-step procedure. For this purpose, protein G from *Streptococcus* sp. (7.5 μL, c = 1 mg mL^{-1}) was bound to 25 μL of carboxylated MF microparticles by 1-ethyl-3-(3-dimethylaminopropyl)carbodiimide. Subsequently, 25 μL of these particles was coated with the mAb HPT-101 (4 μL, c = 2.1 mg mL^{-1}), and the mAb was cross-linked to protein G *via* reaction with dimethyl pimelimidate.

Optical Tweezers Setup and the Experiment. We use an optical tweezers setup similar to the one described in Stangner *et al.*[34] and Wagner *et al.*[35] Our sample cell consists of a stainless steel corpus with a volume of ~80 μL, enclosed by two coverslips on bottom and top. Additionally, to exchange buffer solution, an inlet and outlet are provided. In order to carry out pair interaction

experiments, a micropipet (inner diameter ~0.5 μm) is incorporated into the chamber. The sample cell is mounted on an optical stage that can be moved in three dimensions with nanometer resolution using piezoactuators (P-5173CD, PI, Karlsruhe, Germany). The whole experimental setup is located in a temperature-controlled room at 298 ± 1 K, and all experiments are carried out in PBS solution at pH 7.4.

Position detection is realized with a CCD camera (1M60, Dalsa, Munich, Germany) acquiring 60 frames per second with a spatial resolution in the *xy*-plane of ±2 nm.[36] The image scale is given with 13.25 nm/pixel. Due to drift effects of the micropipet, it is necessary to compensate this movement for long-term stability. For this purpose, height detection is employed to control the position of a microparticle in the *z*-direction with a precision of ±2 nm.[35] Force calibration of the bead in the optical trap is accomplished by displacing the particle from its equilibrium position, and the data are analyzed using Stokes' formula. For the present experiments we obtained a force constant of 0.080 ± 0.003 pN nm^{-1} at a laser power of 200 mW, resulting in a force resolution of ±0.2 pN.

In order to ensure that single bindings are investigated, the surface coverage of the microparticles (coated with either peptides or mAbs) is successively decreased until the number of detectable multiple rupture events is lower than 2% and the distributions of the rupture forces are found to be independent of the coating density (data not shown).[28,34]

Theory. Dynamic force spectroscopy[37,38] provides a method to gain detailed insight into the dynamics of receptor−ligand interactions on a molecular level. For a theoretical description of the following experiments we use the theory of Dudko, Hummer, and Szabo (DHS model),[31] which provides a common framework to rationalize the different results previously obtained independently by the same authors.[39,40] Based on Kramers' transition state theory,[32] the DHS model describes the receptor−ligand pair dissociation as an escape process from a potential well on a 1D free-energy surface. This process is characterized by three parameters: the binding length x_{ts}, the bond lifetime at zero applied force τ_0, and the depth of the binding potential ΔG. It is important to highlight that ΔG is not the free energy for bond formation from which bond affinity can be calculated. Rather, the ΔG value measured by DFS experiments is the free-energy barrier from the (metastable) bound state to the transition state through which the bonds pass during rupture, and its value is connected to the kinetics of bond rupture *via* Kramers' theory. In order to recover information about the bond affinity, *e.g.*, the ΔG value obtained in other experiments such as ELISA tests, which probe the bond thermodynamic stability, one has to supplement information on the kinetics of bond rupture with the data on the kinetics of bond formation; see eqs 4 and 5. Once combined, a proper comparison to results obtained *via* other experimental techniques can be made.

When the effect of an external force is considered, the aforementioned approach results in a force-dependent bond lifetime, $\tau_{DHS}(F)$.[31] For the case of a constant loading rate, the following expression is obtained:

$$\tau_{DHS}(F) = \tau_0\left(1 - \frac{\nu F x_{ts}}{\Delta G}\right)^{1-1/\nu} \times \exp\left\{-\beta\Delta G\left[1 - \left(1 - \frac{\nu F x_{ts}}{\Delta G}\right)\right]^{1/\nu}\right\} \quad (6)$$

in which F is the externally applied force and $\beta = (k_B T)^{-1}$ is the inverse thermal energy. The scaling factor υ specifies the shape of the underlying free-energy landscape. For $\upsilon = 1$ the original results of Bell's phenomenological formula[37] are recovered, whereas $\upsilon = 0.5$ and $\upsilon = 0.66$ correspond to the Hummer, Szabo,[39] and Dudko[40] model, respectively. Using eq 6 it is possible to calculate the theoretical distribution of rupture forces $p(F)$:

$$p(F) = \frac{\exp\left(-\int_0^F [\dot{F}(f)\,\tau(f)]^{-1}\,df\right)}{\dot{F}(F)\,\tau(F)} \quad (7)$$

The error estimation for the three fit parameters in eq 6 follows the instruction outlined in Wagner *et al.*[28] To apply eq 6 to experimental data, it is necessary to convert the rupture force histograms, starting at F_0 and ending at $F_N = F_0 + Nb$ as well as containing N bins with a width of b, into a discrete function $\tau(F)$ by using the following expression (k = 1, 2, 3, ...):

$$\tau(F_0 + (k - 1/2)b) = \frac{(h_k/2 + \sum_{i=k+1}^{N} h_i)b}{h_{k\dot{F}(F_0 + (k - 1/2)b)}} \quad (8)$$

with $h_i = C_i/(N_{tot}b)$, N_{tot} being the total number of rupture events, and C_i being the number of rupture events in each bin. For data sets comprising substantial outliers eq 8 cannot be applied. In such cases, another algorithm to calculate the function $\tau(F)$ is appropriate.[31] Hence, $\tau(\bar{F})$ is calculated for each rupture force histogram by taking the interquartile range $\delta F = F_3 - F_1$ (meaning that 25% of the rupture forces are higher than F_3 and 25% are lower than F_1):

$$\tau(\bar{F}) = \frac{3}{4}\frac{\delta F}{\dot{F}(\bar{F})} \quad (9)$$

with $\bar{F}$ being the median rupture force.

Conflict of Interest: The authors declare no competing financial interest.

Acknowledgment. Financial support by the European Social Fund (ESF), the Free State of Saxony, and BuildMoNa is gratefully acknowledged. Furthermore, we thank Jörg Reinmuth and Viktor Skokow for technical support. S.A.-U. acknowledges financial support from the Alexander von Humboldt Foundation *via* a postdoctoral fellowship. J.D. acknowledges financial support from DFG and the Alexander von Humboldt Foundation.

REFERENCES AND NOTES

1. Köhler, G.; Milstein, C. Continuous Cultures of Fused Cells Secreting Antibody of Predefined Specificity. *Nature* **1975**, *256*, 495–497.
2. Buss, N. A.; Henderson, S. J.; McFarlane, M.; Shenton, J. M.; de Haan, L. Monoclonal Antibody Therapeutics: History and Future. *Curr. Opin. Pharmacol.* **2012**, *12*, 615–622.
3. Casi, G.; Neri, D. Antibody−Drug Conjugates: Basic Concepts, Examples and Future Perspectives. *J. Controlled Release* **2012**, *161*, 422–428.
4. Gerber, H.-P.; Koehn, F. E.; Abraham, R. T. The Antibody-Drug Conjugate: An Enabling Modality for Natural Product-Based Cancer Therapeutics. *Nat. Prod. Rep.* **2013**, *30*, 625.
5. Lin, K.; Tibbitts, J. Pharmacokinetic Considerations for Antibody Drug Conjugates. *Pharm. Res.* **2012**, *29*, 2354–2366.
6. Nelson, A. L.; Dhimolea, E.; Reichert, J. M. Development Trends for Human Monoclonal Antibody Therapeutics. *Nat. Rev. Drug Discovery* **2010**, *9*, 767–774.
7. Reichert, J. M.; Dhimolea, E. The Future of Antibodies as Cancer Drugs. *Drug Discovery Today* **2012**, *17*, 954–963.
8. Reichert, J. M. Antibodies to Watch in 2013: Mid-Year Update. *mAbs* **2013**, *5*.
9. Ducry, L.; Stump, B. Antibody−Drug Conjugates: Linking Cytotoxic Payloads to Monoclonal Antibodies. *Bioconjugate Chem.* **2009**, *21*, 5–13.
10. Singer, D.; Lehmann, J.; Hanisch, K.; Härtig, W.; Hoffmann, R. Neighbored Phosphorylation Sites as PHF-Tau Specific Markers in Alzheimer's Disease. *Biochem. Biophys. Res. Commun.* **2006**, *346*, 819–828.
11. Borrebaeck, C. A. K. Antibodies in Diagnostics − From Immunoassays to Protein Chips. *Immunol. Today* **2000**, *21*, 379–382.
12. Cahill, D. J. Protein and Antibody Arrays and their Medical Applications. *J. Immunol. Methods* **2001**, *250*, 81–91.
13. Hernández, F.; Avila, J. Tauopathies. *Cell. Mol. Life Sci.* **2007**, *64*, 2219–2233.
14. Schaap, I. A. T.; Hoffmann, B.; Carrasco, C.; Merkel, R.; Schmidt, C. F. Tau Protein Binding Forms a 1 nm Thick

Layer along Protofilaments without Affecting the Radial Elasticity of Microtubules. *J. Struct. Biol.* **2007**, *158*, 282–292.
15. Wiltfang, J.; Lewczuk, P.; Riederer, P.; Grünblatt, E.; Hock, C.; Scheltens, P.; Hampel, H.; Vanderstichele, H.; Iqbal, K.; Galasko, D.; *et al*. Consensus Paper of the WFSBP Task Force on Biological Markers of Dementia: The Role of CSF and Blood Analysis in the Early and Differential Diagnosis of Dementia. *World J. Biol. Psychiatry* **2005**, *6*, 69–84.
16. Matthes, D.; Gapsys, V.; Daebel, V.; de Groot, B.L. Mapping the Conformational Dynamics and Pathways of Spontaneous Steric Zipper Peptide Oligomerization. *PLoS One* **2011**, *6*, e19129 EP -.
17. Mukrasch, M. D.; Markwick, P.; Biernat, J.; von Bergen, M.; Bernadó, P.; Griesinger, C.; Mandelkow, E.; Zweckstetter, M.; Blackledge, M. Highly Populated Turn Conformations in Natively Unfolded Tau Protein Identified from Residual Dipolar Couplings and Molecular Simulation. *J. Am. Chem. Soc.* **2007**, *129*, 5235–5243.
18. Eidenmüller, J.; Fath, T.; Maas, T.; Pool, M.; Sontag, E.; Brandt, R. Phosphorylation-Mimicking Glutamate Clusters in the Proline-Rich Region Are Sufficient to Simulate the Functional Deficiencies of Hyperphosphorylated Tau Protein. *Biochem. J.* **2001**, *357*, 759–767.
19. Haase, C.; Stieler, J. T.; Arendt, T.; Holzer, M. Pseudophosphorylation of Tau Protein Alters its Ability for Self-Aggregation. *J. Neurochem.* **2004**, *88*, 1509–1520.
20. Tomoo, K.; Yao, T.-M.; Minoura, K.; Hiraoka, S.; Sumida, M.; Taniguchi, T.; Ishida, T. Possible Role of Each Repeat Structure of the Microtubule-Binding Domain of the Tau Protein in *in Vitro* Aggregation. *J. Biochem.* **2005**, *138*, 413–423.
21. Zhou, L.-X.; Zeng, Z.-Y.; Du, J.-T.; Zhao, Y.-F.; Li, Y.-M. The Self-Assembly Ability of the First Microtubule-Binding Repeat from Tau and Its Modulation by Phosphorylation. *Biochem. Biophys. Res. Commun.* **2006**, *348*, 637–642.
22. Moreno-Herrero, F.; Valpuesta, J. M.; Pérez, M.; Colchero, J.; Barö, A. M.; Avila, J.; de Garcini, E.M. Characterization by Atomic Force Microscopy and Cryoelectron Microscopy of Tau Polymers Assembled in Alzheimer's Disease. *J. Alzheim. Dis.* **2001**, *3*, 443–451.
23. Barrantes, A.; Sotres, J.; Hernando-Pérez, M.; Benítez, M. J.; de Pablo, P. J.; Baró, A. M.; Ávila, J.; Jiménez, J. S. Tau Aggregation Followed by Atomic Force Microscopy and Surface Plasmon Resonance, and Single Molecule Tau-Tau Interaction Probed by Atomic Force Spectroscopy. *J. Alzheim. Dis.* **2009**, *18*, 141–151.
24. Singer, D.; Herth, N.; Kuhlmann, J.; Holland-Nell, K.; Beck-Sickinger, A. G.; Hoffmann, R. Mapping of Phosphorylation-Dependent Anti-Tau Monoclonal Antibodies in Immunoblots Using Human Tau-Constructs Synthesized by Native Chemical Ligation. *Biochem. Biophys. Res. Commun.* **2008**, *367*, 318–322.
25. Florin, E.; Moy, V.; Gaub, H. Adhesion Forces between Individual Ligand-Receptor Pairs. *Science* **1994**, *264*, 415–417.
26. Merkel, R.; Nassoy, P.; Leung, A.; Ritchie, K.; Evans, E. Energy Landscapes of Receptor-Ligand Bonds Explored with Dynamic Force Spectroscopy. *Nature* **1999**, *397*, 50–53.
27. Schwesinger, F. Unbinding Forces of Single Antibody-Antigen Complexes Correlate with their Thermal Dissociation Rates. *Proc. Natl. Acad. Sci. U.S.A.* **2000**, *97*, 9972–9977.
28. Wagner, C.; Singer, D.; Ueberschär, O.; Stangner, T.; Gutsche, C.; Hoffmann, R.; Kremer, F. Dynamic Force Spectroscopy on the Binding of Monoclonal Antibodies and Tau Peptides. *Soft Matter* **2011**, *7*, 4370.
29. Robert, P.; Benoliel, A.-M.; Pierres, A.; Bongrand, P. What Is the Biological Relevance of the Specific Bond Properties Revealed by Single-Molecule Studies? *J. Mol. Recognit.* **2007**, *20*, 432–447.
30. Scott, D. W. On Optimal and Data-Based Histograms. *Biometrika* **1979**, *66*, 605–610.
31. Dudko, O. K.; Hummer, G.; Szabo, A. Theory, Analysis, and Interpretation of Single-Molecule Force Spectroscopy Experiments. *Proc. Natl. Acad. Sci. U.S.A.* **2008**, *105*, 15755–15760.
32. Kramers, H. A. Brownian Motion in a Field of Force and the Diffusion Model of Chemical Reactions. *Physica* **1940**, *7*, 284–304.
33. Daly, N. L.; Hoffmann, R.; Otvos, L.; Craik, D. J. Role of Phosphorylation in the Conformation of τ Peptides Implicated in Alzheimer's Disease. *Biochemistry* **2000**, *39*, 9039–9046.
34. Stangner, T.; Singer, D.; Wagner, C.; Gutsche, C.; Ueberschär, O.; Hoffmann, R.; Kremer, F. FACS-Sorted Particles Reduce the Data Variance in Optical Tweezers-Assisted Dynamic Force Spectroscopy Measurements. *Phys. Biol.* **2013**, *10*, 46004.
35. Wagner, C.; Stangner, T.; Gutsche, C.; Ueberschär, O.; Kremer, F. Optical Tweezers Setup with Optical Height Detection and Active Height Regulation under White Light Illumination. *J. Opt.* **2011**, *13*, 115302.
36. Ueberschär, O.; Wagner, C.; Stangner, T.; Gutsche, C.; Kremer, F. A Novel Video-Based Microsphere Localization Algorithm for Low Contrast Silica Particles under White Light Illumination. *Opt. Laser Eng.* **2012**, *50*, 423–439.
37. Bell, G. Models for the Specific Adhesion of Cells to Cells. *Science* **1978**, *200*, 618–627.
38. Evans, E.; Ritchie, K. Dynamic Strength of Molecular Adhesion Bonds. *Biophys. J.* **1997**, *72*, 1541–1555.
39. Hummer, G.; Szabo, A. Kinetics from Nonequilibrium Single-Molecule Pulling Experiments. *Biophys. J.* **2003**, *85*, 5–15.
40. Dudko, O. K.; Filippov, A. E.; Klafter, J.; Urbakh, M. Beyond the Conventional Description of Dynamic Force Spectroscopy of Adhesion Bonds. *Proc. Natl. Acad. Sci. U.S.A.* **2011**, *100*, 11378–11381.
41. Lomax, R. G.; Hahs-Vaughn, D. L. *Statistical Concepts: A Second Course*, 4th ed.; Routledge Academic: New York, NY, 2012.